https://doi.org/10.5194/egusphere-2026-4858
Preprint. Discussion started: 22 September 2026
© Author(s) 2026. CC BY 4.0 License.

Dual-band information helps constrain canopy water content and temperature retrievals from vegetation optical depth

Yitong Yao[1,2*], Vincent Humphrey[3], Alexandra G. Konings[4], Jeffrey D. Wood[5], Yujie Wang[2], Ke Liu[2], Dien Wu[2], Christian Frankenberg[2,6]

[1] Institute of Environment and Ecology, Tsinghua Shenzhen International Graduate School, Shenzhen, 518071, China
[2] Division of Geological and Planetary Sciences, California Institute of Technology, Pasadena, CA 91125, USA
[3] Federal Office of Meteorology and Climatology MeteoSwiss, Zürich, CH-8058, Switzerland
[4] Department of Earth System Science, Stanford University, Stanford, CA 94305, USA
[5] School of Natural Resources, University of Missouri, Columbia, MO 65211, USA
[6] Jet Propulsion Laboratory, California Institute of Technology, Pasadena, CA 91109, USA

Correspondence to: Yitong Yao (yitongyao@sz.tsinghua.edu.cn)

Abstract. Vegetation canopy water content and temperature fundamentally control plant physiology. They usually have strong diurnal cycles with substantial variations on the hourly basis. However, due to the scarcity of high-frequency observations, a major obstacle has long been existing in deciphering the plant hydrodynamics. Vegetation Optical Depth (VOD) provides a promising satellite and ground-based proxy by quantifying microwave attenuation by canopy liquid water, but it co-varies with biomass and temperature. Temperature-dependent dielectric effects also complicate the isolation of water dynamics. To assess the information extent that can be inferred from VOD and to assess the contribution of a second wavelength (as available with Global Navigation Satellite System, GNSS) in disentangling influences from multiple processes, we developed a Bayesian inversion framework coupled to a semi-empirical electromagnetic model to retrieve canopy water content (M_g), vegetation volume, and canopy temperature from single- and dual-frequency data using both theoretical sensitivity analyses and GNSS observations. After testing with simulated VOD at two GNSS bands (1.575 and 1.176 GHz), we applied the method to in situ GNSS-based VOD and evaluated against field measurements. Simulations indicate that single-band VOD with 0.5–4% measurement error already constrains M_g and vegetation volume. Adding a second band substantially improves temperature retrievals, reducing posterior uncertainty to 2.3K, although the benefit declines rapidly as VOD errors grow. When applied to observations, incorporating scaled leaf area index as an additional constraint improves the M_g-leaf water potential relationship, underscoring the value of auxiliary information. Through a first direct comparison of the information provided by mono-band and dual-band, our results show that converting VOD into biophysical variables is strengthened by dual-frequency information and complementary constraints, emphasizing the need for additional validation to robustly retrieve canopy water content and temperature at high frequency.

https://doi.org/10.5194/egusphere-2026-4858
Preprint. Discussion started: 22 September 2026
© Author(s) 2026. CC BY 4.0 License.

1 Introduction

Plant water content is integral to many physiological processes and provides a key indicator of vegetation responses to environmental stress. Water deficits induced by extreme climate events threaten the land's carbon sink capacity (Piao et al., 2019; Reichstein et al., 2013), leading to tree mortality (Rao et al., 2019) and heightened wildfire risk (Rao et al., 2022). Therefore, understanding plant water content dynamics is fundamental for identifying terrestrial ecosystem vulnerability.

Microwave remote sensing is particularly promising for measuring vegetation water content because it provides large-scale coverage and is less affected by nighttime and cloudy conditions compared to optical remote sensing. Microwave observations of vegetation water content are typically expressed as vegetation optical depth (VOD), which is defined as the integral of extinction coefficients across vegetation canopy layers in the microwave domain. Ground-based measurements have demonstrated a close relationship between VOD and canopy water content (Jackson and Schmugge, 1991). Because VOD integrates the water stored throughout the canopy, its magnitude is influenced by both vegetation biomass and relative water content (Konings et al., 2019). Consequently, VOD has been widely used to investigate vegetation biomass (Yang et al., 2023), terrestrial carbon dynamics (Fan et al., 2019; Wigneron et al., 2024), phenology (Tian et al., 2018), plant hydraulic traits (Liu et al., 2021), drought (Kumar et al., 2021), and wildfire risk (Fan et al., 2023; Forkel et al., 2023).

Despite its prevailing applications, interpreting VOD remains challenging because its magnitude is jointly controlled not only by vegetation water content and biomass, but also by canopy temperature, water salinity, and microwave wavelength (Ulaby and Long, 2014). Retrieving these individual components from VOD constitutes a fundamentally ill-posed inverse problem. While biomass and relative water content have long been recognized as major controls on VOD (Konings et al., 2019), recent studies show that temperature also exerts a non-negligible influence by altering the dielectric properties of vegetation water (Zhao et al., 2024). Water salinity further modifies dielectric losses through its effect on ionic conductivity, and both temperature and salinity sensitivities vary with microwave wavelength (Ulaby and Long, 2014). As a result, changes in VOD cannot be uniquely attributed to vegetation water content without accounting for additional influences.

Growing observational and modelling evidence demonstrates the importance of temperature in VOD interpretation. Around the freeze-thaw transition, VOD increases with temperature and reaches a maximum near 0 °C because of water-ice phase transitions (Roy et al., 2020), complicating the interpretation of springtime VOD increases in boreal ecosystems (Schwank et al., 2021). Under warm conditions, increasing temperature enhances dielectric losses in saline vegetation water through changes in ionic conductivity (Ulaby and Long, 2014). During heatwaves, temperature has been shown to substantially modify the interpretation of VOD dynamics under water stress (Humphrey and Frankenberg, 2023). Furthermore, simulation studies using electromagnetic models have demonstrated that temperature contributes significantly to diurnal VOD variations across both L-band and X-band frequencies (Zhao et al., 2024). Because elevated temperatures are typically accompanied by declining vegetation water content through enhanced evaporative demand, neglecting temperature effects may lead to biased estimates of vegetation water status during compound heat and drought events.

https://doi.org/10.5194/egusphere-2026-4858
Preprint. Discussion started: 22 September 2026
© Author(s) 2026. CC BY 4.0 License.

Beyond its confounding influence on VOD retrieval, canopy temperature is itself an ecologically important state variable. The difference between canopy and air temperature reflects vegetation thermal regulation and strongly influences stomatal conductance and photosynthesis (Novick et al., 2024; Still et al., 2022). Accurate retrieval of canopy temperature would therefore improve both the interpretation of VOD and our understanding of vegetation physiological responses to environmental stress.

Although VOD depends simultaneously on vegetation volume, water content, and canopy temperature, these variables evolve over different temporal scales. Vegetation structure and biomass generally vary over seasonal to annual timescales, whereas relative water content and canopy temperature fluctuate rapidly over hours in response to transpiration and atmospheric forcing. This temporal separation suggests that high-frequency observations may provide additional information for disentangling these processes (Konings et al., 2021b), although current spaceborne microwave missions cannot provide continuous diurnal observations.

A promising alternative is offered by ground-based Global Navigation Satellite System (GNSS) observations. By measuring the attenuation of GNSS signals using receivers positioned above and below the canopy, GNSS provides continuous, robust, and cost-effective measurements of VOD that resolve both seasonal and diurnal dynamics (Humphrey and Frankenberg, 2023). Previous studies have demonstrated that hourly GNSS VOD captures rapid changes in vegetation water content while simultaneously tracking slower seasonal biomass variations (Humphrey and Frankenberg, 2023; Yao et al., 2024). In addition to their high temporal resolution, GNSS observations provide measurements at multiple closely spaced frequencies (L1 and L5). Because the dielectric response of vegetation water exhibits wavelength-dependent temperature sensitivity (Ulaby and Long, 2014) while the two frequencies sample nearly the same vegetation canopy, dual-band observations may provide additional independent information for separating canopy temperature from vegetation water content and vegetation volume. Whether this additional information is sufficient to overcome the ill-posed nature of VOD inversion, however, remains unknown and deserves investigation.

Here, we leverage recent advances in GNSS-based VOD measurements at the MOFLUX site (Humphrey and Frankenberg, 2023; Yao et al., 2024) to investigate the information content of mono-band and dual-band observations. We hypothesize that the additional temperature sensitivity provided by dual-frequency measurements can improve retrievals of canopy temperature and thereby reduce ambiguity in estimates of vegetation water content and vegetation volume. To test this hypothesis, we combined a semi-empirical electromagnetic model with a Bayesian inversion framework and addressed two questions: (1) To what extent can mono-band and dual-band VOD constrain vegetation water content, canopy temperature, and vegetation volume? (2) Does the additional information provided by a second frequency translate into improved retrieval performance under realistic observational uncertainties? We first evaluate these questions using synthetic observing system simulation experiments, and then apply the retrieval framework to GNSS observations at the MOFLUX site. Finally, we compare the retrieved variables against independent field measurements and examine wavelength-dependent temperature sensitivity using observations from the L1 and L5 GNSS bands.

https://doi.org/10.5194/egusphere-2026-4858
Preprint. Discussion started: 22 September 2026
© Author(s) 2026. CC BY 4.0 License.

2 Materials and Methods

2.1 Retrieval framework

We evaluated the information content of mono-band and dual-band VOD observations using two complementary experiments (Figure 1). First, an Observing System Simulation Experiment (OSSE) was conducted to quantify the theoretical ability of VOD observations to constrain vegetation water content (M_g), canopy temperature (T_c), and vegetation volume (V_{veg}) under controlled conditions. Second, the same retrieval framework was applied to GNSS VOD observations collected at a flux tower site (i.e., MOFLUX) and evaluated against independent field measurements. Both experiments use the same electromagnetic forward model and Bayesian inversion framework. The OSSE provides the theoretical upper limit of retrieval performance, whereas the application to GNSS observations assesses retrieval performance under realistic measurement uncertainties. Figure 1 summarizes the workflow. Detailed methods for each experiment are provided below.

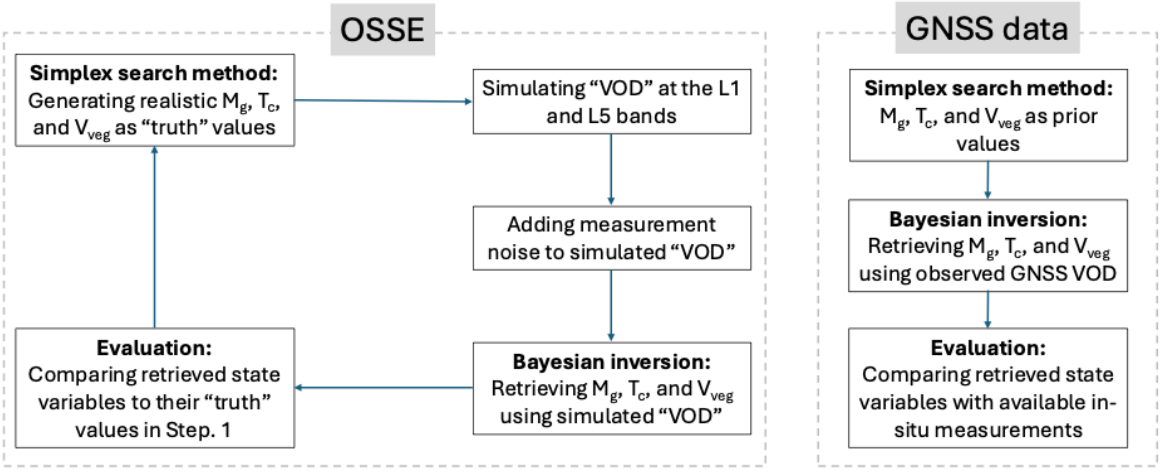

Figure 1. Schematic illustrating the experiment setup of Observing System Simulation Experiment (OSSE) and retrieval using GNSS data.

2.2 Study site and observations

2.2.1 Study site

The experiment was conducted at the MOFLUX site, situated in central Missouri, USA (38.7°N 92.2°W; AmeriFlux ID US-MOz). This area falls within the warm, humid, and continental climate zones, with a mean annual temperature of 13°C and a mean annual precipitation of 1,140 mm. The forest is predominantly oak-hickory, with important tree species including white oak, black oak, sugar maple, shagbark hickory, eastern red cedar and white ash, which are routinely measured for predawn leaf water potential (Wood et al., 2023). This drought-prone site frequently experiences late summer water stress, as

https://doi.org/10.5194/egusphere-2026-4858
Preprint. Discussion started: 22 September 2026
© Author(s) 2026. CC BY 4.0 License.

indicated by periodic leaf water potential measurements (Gu et al., 2016, 2015). The average tree height ranges from 17 to 20 m. Regular predawn leaf water potential ($\psi_{pd,l}$) measurements began in 2004, and are conducted on a weekly to bi-weekly basis during the growing season to assess community water status. Leaf area index (LAI) measurements were also obtained at weekly to bi-weekly intervals (Wood et al., 2022). For this study, we also used half-hourly air temperature and soil moisture content measurements.

2.2.2 GNSS VOD observations

Two Septentrio PolaRx5e GNSS receivers equipped with PolaNt-x MF right-hand circular polarized (RHCP) GNSS antennas were deployed at the Ozark AmeriFlux (MOFLUX) site in Missouri, USA to measure multi-constellation GNSS signals. One receiver was positioned above the forest canopy as an open-sky reference, while the other receiver was placed beneath to measure the attenuation by vegetation. Using the signal-to-noise ratios (SNR) from both GNSS receivers, we derived the canopy VOD following the method outlined in Humphrey and Frankenberg (2023). Notably, the number of satellites tracking both L1 and L5 bands simultaneously is less than 50% of those tracking the L1 band only (Figure S1 in the Supplement). This dataset spans from April 2021 to December 2022, providing GNSS VOD observations on an hourly basis. We retrieved VOD from two GNSS bands: the L1 band (1.575 GHz) and L5 band (1.176 GHz).

2.3 Canopy electromagnetic forward model

The retrieval framework relies on a forward model that links canopy properties to observed VOD. We used a semi-empirical electromagnetic model to simulate VOD as a function of vegetation water content, canopy temperature, vegetation volume, wavelength, and water salinity. This forward model serves as the observation operator in the Bayesian inversion described below. Specifically, a dielectric mixing model of canopy transmissivity was used to explore the potential roles of water content, temperature, and vegetation volume in influencing VOD magnitudes. We employed a relatively simple formulation that considers only the attenuating effect of the canopy on the direct signal power and represents the canopy as a homogeneous layer consisting of randomly distributed elements (Humphrey & Frankenberg, 2023). This homogeneous-canopy assumption, used when independent constraints to separate leaf and woody contributions are unavailable, has been employed in previous studies (Chaparro et al., 2024; Jagdhuber et al., 2025). VOD is expressed as a function of a bulk canopy extinction coefficient (K_e) and tree height (h) in Eq. 1.

$$VOD = 2k_e h \tag{1}$$

The factor "2h" in Eq. 1 represents the total path length of radiation through vegetation, where h is the canopy height. By neglecting scattering effects, the extinction coefficient is further linked to the complex index of refraction of the canopy layer (Eq. 2).

$$k_e = \frac{2\pi}{\lambda_0} n_c'' \tag{2}$$

https://doi.org/10.5194/egusphere-2026-4858
Preprint. Discussion started: 22 September 2026
© Author(s) 2026. CC BY 4.0 License.

where λ_0 is wavelength.

The complex index of refraction (n_c'') is in turn calculated from the dielectric constant of the canopy layer (ϵ_c, Eq. 3).

$$n_c'' = -Im\{\sqrt{\epsilon_c}\} \quad (3)$$

A two-phase refractive mixing approach was used to calculate ϵ_c (Eq. 4).

$$\sqrt{\epsilon_c} = V_{veg}\sqrt{\epsilon_{veg}} + (1 - V_{veg})\sqrt{\epsilon_{air}} \quad (4)$$

where V_{veg} is vegetation volume.

Assuming negligible dielectric loss in the air (ϵ_{air}), n_c'' is mainly determined by the dielectric constant of vegetation (ϵ_{veg}) as shown in Eq. 5.

$$n_c'' = -Im\{\sqrt{\epsilon_{veg}}\}V_{veg} \quad (5)$$

The dielectric constant of vegetation (ϵ_{veg}) consists of real ($\epsilon_{veg}{}'$) and imaginary parts ($\epsilon_{veg}{}''$), representing the dielectric permittivity and the dielectric loss, respectively (Eq. 6).

$$\epsilon_{veg} = \epsilon_{veg}{}' - i\epsilon_{veg}{}'' \quad (6)$$

Combining Eqs. (1-5) yields:

$$VOD = 2\frac{2\pi}{\lambda_0}[-Im\{\sqrt{\epsilon_{veg}}\}]V_{veg}h \quad (7)$$

VOD is therefore influenced by various factors, with the most important being vegetation water content, canopy temperature, ionic conductivity, and wavelength. We used a semi-empirical model for vegetation dielectric constants (Ulaby & El-rayes ,1987), expressing $\epsilon_{veg}{}'$ and $\epsilon_{veg}{}''$ as functions of gravimetric moisture, temperature, and water salinity (Text S1).

2.4 Initial parameter estimation with simplex optimization

The Bayesian inversion requires realistic prior estimates of M_g, V_{veg}, and water salinity. We therefore first performed an unconstrained optimization using the Nelder–Mead simplex algorithm (Lagarias et al., 1998) to identify parameter combinations that best reproduce the observed GNSS VOD. Specifically, following the retrieval algorithm outlined in Humphrey & Frankenberg (2023), we estimated M_g and V_{veg} using GNSS VOD observations at the L1 band. The root mean squared error (RMSE) between the modeled and observed VOD was used as cost function. The simplex search method, designed to find the minimum of an unconstrained multivariate function, was used to optimize M_g and V_{veg} within a search space spanning a range of plant water salinity values (from 1 to 15 psu). This is a direct search method that does not use numerical or analytic gradients. During this process, T_c was assumed to be known and was represented by air temperature

https://doi.org/10.5194/egusphere-2026-4858
Preprint. Discussion started: 22 September 2026
© Author(s) 2026. CC BY 4.0 License.

inputs. The salinity value that minimizes the cost function was selected as the optimal value. The V_{veg} time series was smoothed using a low-pass filter to remove high-frequency variations, as vegetation volume is not expected to change rapidly over short periods. The smoothed V_{veg} was then used as a constraint to derive a new M_g and this M_g time series was itself subsequently smoothed using a low-pass filter to eliminate high-frequency noise. These optimized fields serve two purposes that (1) they provide the synthetic "truth" used in the OSSE, and (2) they provide prior estimates for the Bayesian inversion applied to GNSS observations.

2.5 Bayesian inversion

Retrieval of M_g, T_c, and V_{veg} from VOD constitutes an underdetermined inverse problem because multiple vegetation properties simultaneously influence microwave attenuation. We adopted a Bayesian inversion framework, which combines prior information with VOD observations while explicitly accounting for uncertainties in both. The Bayesian framework is used consistently in both the OSSE and the retrieval from GNSS observations (Dutta et al., 2019; Liu et al., 2024). We solved for the posterior estimates of M_g, T_c, and V_{veg} at each time step. The cost function used in Bayesian inversion extends the concept of minimizing the root mean squared error by considering information from both prior assumptions as well as measurements, both with respective uncertainties. The cost function J(x) for this problem is defined in Eq. (8).

$$J(x) = \gamma(y - Kx)^T S_\varepsilon^{-1}(y - Kx) \; + \; (x - x_a)^T S_a^{-1}(x - x_a) \tag{8}$$

where x is a vector representing the optimized estimates of hourly M_g, T_c, and daily V_{veg}. The x_a vector represents the *a priori* estimates of these variables. The vector y consists of the observed VOD from either the L1 band alone (mono-band) or both L1 and L5 bands (dual-band). The error covariance matrices for the *a priori* state vector (S_a) and observations (S_ε) are represented by diagonal matrices, with the diagonal elements corresponding to the error variance of the retrieved variables and the error variance of the observations at each time step, respectively. All off-diagonal elements are set to zero, assuming the errors are uncorrelated with each other. The matrix K is the Jacobian matrix of the electromagnetic model, representing the derivatives of the VOD with respect to our state vector elements. Lastly, γ is a regularization factor to balance the observational VOD error (the first term of Eq. 8) and the *a priori* error (the second term of Eq. 8). It acts to stabilize the non-linear inversion, which is performed using the Levenberg-Marquardt (LM) approach (Levenberg, 1944; Marquardt, 1963; Rodgers, 2000). We used the analytical solution for $\frac{\partial J}{\partial x} = 0$ to obtain the optimal estimates of the posterior state x_{i+1} as follows (Eq. 9). The subscript i refers to the iteration step.

$$x_{i+1} = x_i + ((1+\gamma)S_a^{-1} + K_i^T S_\epsilon^{-1} K_i)^{-1}(K_i^T S_\epsilon^{-1}[y - F(x_i)] - S_a^{-1}[x_i - x_a]) \tag{9}$$

The posterior uncertainty is computed as:

$$\hat{S} = (K_i^T S_\epsilon^{-1} K_i + S_a^{-1})^{-1} \tag{10}$$

https://doi.org/10.5194/egusphere-2026-4858
Preprint. Discussion started: 22 September 2026
© Author(s) 2026. CC BY 4.0 License.

A theoretical uncertainty reduction (UR) for state variables is computed for M_g, T_c, and V_{veg} separately as Eq .(11).

$$UR = 1 - \frac{\hat{\sigma}}{\sigma_a} \quad (11)$$

where $\hat{\sigma}$ and σ_a are the standard deviation of the posterior and prior error in the state variables, the square root of diagonal elements in $\hat{S}$ and S_a. The UR is used to show the performance of mono-band and dual-band retrievals in terms of uncertainty reduction.

The Bayesian inversion was conducted at a daily time step. In the mono-band case, the vector y comprises 24 hourly VOD measurement values from the L1 band per day. $F(x_i)$ is composed of VOD computations from the electromagnetic model at the L1 band. In the dual-band case, the vector y is composed of 48 hourly VOD measurement values from both the L1 and L5 bands per day. $F(x_i)$ is composed of VOD computations from the electromagnetic model at the L1 and L5 bands. For the mono-band retrieval, the posterior estimate, the last step of x_{i+1}, $\hat{x}$, is a 49 element vector with the first 24 elements representing the posterior T_c for each hour of the day, the next 24 elements representing the posterior hourly M_g, and the final element representing the posterior daily V_{veg}. We used the first-step retrievals as priors for M_g and V_{veg}, and T_{air} as the prior for T_c .

The averaging kernel matrix $A=\partial\hat{x}/\partial x$, represents the sensitivity of the maximum a posteriori probability solution ($\hat{x}$) to the true state x and will be used to analyze the sensitivity of our solutions to prior information and observation constraints. The matrix A is calculated as the product of the gain matrix $G=\partial\hat{x}/\partial y$ and the Jacobian matrix $K=\partial y/\partial x$:

$$G = (K^T S_\epsilon^{-1} K + S_a^{-1})^{-1} K^T S_\epsilon^{-1} \quad (12)$$

$$A = GK = (K^T S_\epsilon^{-1} K + S_a^{-1})^{-1} K^T S_\epsilon^{-1} K \quad (13)$$

2.6 Observing System Simulation Experiment (OSSE)

2.6.1 Generation of synthesis truth dataset in OSSE

The purpose of the OSSE is to quantify the theoretical information content of mono-band and dual-band VOD observations under controlled conditions, where the true canopy state is known. This experiment isolates the effects of measurement uncertainty and observation configuration from other sources of error present in real observations. The optimized M_g and V_{veg} time series obtained from the simplex optimization described in Section 2.4 were used as realistic synthetic truth states for the OSSE. The electromagnetic model (Section 2.3) was then used to generate synthetic truth VOD datasets at the L1 and L5 bands. These M_g and V_{veg} datasets were then used as the "truth" to evaluate retrieval performance in OSSE.

2.6.2 Experiment design

To compare the performance of mono-band and dual-band retrieval scenarios, we conducted an OSSE. This approach involves testing retrieval algorithms on simulated, yet realistic, ground-based observations to assess the accuracy of inferred results. The goal of the OSSE in this context is to quantitatively evaluate the extent to which VOD measurements can constrain the estimates of M_g, T_c, and V_{veg} in both mono-band and dual-band scenarios. We conducted the OSSE simulations under

https://doi.org/10.5194/egusphere-2026-4858
Preprint. Discussion started: 22 September 2026
© Author(s) 2026. CC BY 4.0 License.

various conditions, incorporating one or two VOD bands and/or different levels of VOD errors, as detailed below. The steps in our OSSE are summarized in Figure 1.

The motivation for using dual-band data lies in the wavelength-dependent behavior illustrated in Figure 2. The electromagnetic model shows that the fractional VOD changes per degree of temperature change differ between the L1 and L5 bands across varying temperature and M_g ranges. These distinct responses are likely to provide additional constraints when incorporating an additional closely-spaced band.

We began by running the electromagnetic model using M_g, T_c, and V_{veg} values derived from Section 2.4 as realistic input fields to generate a simulated VOD time series at the L1 and L5 bands. Specifically, with T_{air} from the MOFLUX site as the input for T_c, we used the simplex search method to optimize M_g and V_{veg} using GNSS VOD at the L1 band as constraints. We do not optimize T_c here because joint hourly optimization of T_c and M_g is too ill-conditioned in this framework. The observed T_{air} and the optimized, smoothed values of M_g and V_{veg} were then used as inputs to the electromagnetic model to produce synthetic VOD observations. The M_g, T_c, and V_{veg} inputs were treated as the true values, and the VOD generated by the electromagnetic model served as a synthetic "truth" scenario for subsequent analysis.

Mono-band and dual-band retrievals were tested separately. The prior for T_c was set to the true T_c value minus 4°C, based on the observation that the air-canopy temperature difference at our site generally falls within 4 °C (Figure S2). The prior for M_g was estimated at 0.5 g g^{-1} (a typical value for M_g). and the prior for V_{veg} was set to its growing season average. The uncertainty in M_g was defined as 0.2 g g^{-1}, or 40% of the prior value, and the uncertainty in V_{veg} was set at 30% of its seasonal average. To replicate realistic observational noise, Gaussian white noise was added to the pseudo-truth of the simulated VOD, with measurement uncertainties ranging from 0.5% to 4% in increments of 0.5%. The resulting noisy VOD data were input into the Bayesian inversion algorithm (as described in Section 2.5) to estimate the posterior values of M_g, T_c, and V_{veg}. These estimates were compared to the original assumed truth, and the Percent of Uncertainty Reduction was used to quantify the effectiveness of VOD observations from mono-band and dual-band approaches in constraining these key components (Section 2.5). The experiment was repeated 100 times to minimize the impact of the specific randomized errors drawn in any given ensemble member.

https://doi.org/10.5194/egusphere-2026-4858
Preprint. Discussion started: 22 September 2026
© Author(s) 2026. CC BY 4.0 License.

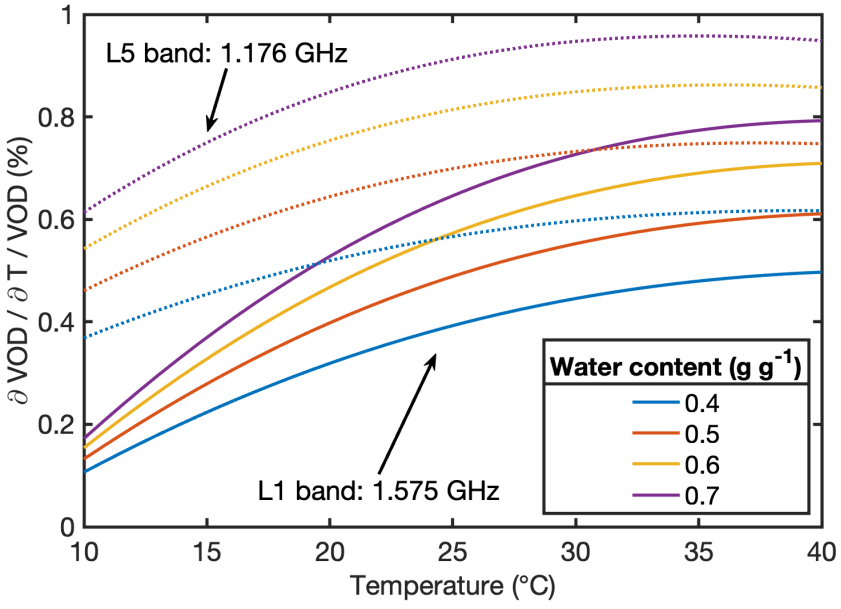

Figure 2. The fractional changes in VOD per degree of temperature change across different temperature and M_g levels. The VOD values in this plot are simulated using the electromagnetic model. Two frequency bands are represented: solid lines for the L1 band and dashed lines for the L5 band.

2.7 Retrieval using GNSS observations

2.7.1 Mono-band and dual-band retrieval setup using GNSS VOD

After evaluating the performance of mono-band and dual-band retrievals using the OSSE, we applied the Bayesian inversion analysis to observed GNSS VOD measurements at MOFLUX. To estimate measurement error, we computed the standard deviation of VOD taken over five consecutive early morning hours, assuming this period represents a relatively stable water content state with balanced water demand and supply, which would imply that the temporal variation is mostly due to observational noise. The measurement error was defined as the ratio of the standard deviation to the mean VOD over this period. During the growing season, the VOD measurements showed an error of ~4%, which we adopted as the measurement error (i.e. S_ε in Eq. 8). T_{air} was used as the prior for T_c, with its error set to 4 °C. We thus implicitly assume that T_{air} is far more readily available than T_c. The priors for M_g and V_{veg} (i.e. the components of x_a in Eq. 9) were obtained from the simplex search method in Section 2.4 and their errors were set to 30% of their respective values, representing a less conservative error estimate (i.e. S_a in Eq. 9).

https://doi.org/10.5194/egusphere-2026-4858
Preprint. Discussion started: 22 September 2026
© Author(s) 2026. CC BY 4.0 License.

2.7.2 Scaling factor

In the dual-band case using real GNSS VOD data, an additional scaling factor (β) is optimized to account for the magnitude mismatch between the electromagnetic model's estimate and GNSS observations at the L5 band (Eq. 14). Theoretically, as shown in Eq. (7), when all other terms remain constant, such as when microwave signals at the L1 and L5 bands are attenuated by the same canopy, longer wavelengths are expected to produce lower VOD values, while shorter wavelengths yield higher VOD values. This implies that VOD at the L5 band should be lower than that at the L1 band. However, in the GNSS VOD data, the observed VOD at the L5 band is higher than that at the L1 band (Figure S3). To address this mismatch, we applied a scaling factor to account for potential underlying causes, including differences in power and signal characteristics dependent on the transmitting satellites, factors that are not accounted for in the current electromagnetic models. The scaling factor can be applied to data from either the L1 band or the L5 band. In this study, we applied the scaling factor (β) to the simulated VOD at the L5 band, where the scaling factor was optimized (Eq. 14).

$$VOD_{sim,L5} = VOD_{EM,L5} \times \beta \quad (14)$$

$VOD_{EM,L5}$ denotes the VOD predicted by the EM model at the L5 band. $VOD_{sim,L5}$ is simulated VOD after adjusting for the magnitude mismatch.

2.7.3 Evaluation against field measurements

After retrieving M_g from GNSS VOD, we examined its correlation with $\psi_{pd,l}$. For the retrieved T_c, we compared it to surface temperature estimates inverted from outgoing long-wave radiation. The retrieved V_{veg} was validated against field measurements of LAI. The measurements are taken every week to two weeks. To determine daily LAI, we linearly interpolated the time series and applied a Savitzky-Golay filter to smooth the resulting time series.

In order to evaluate the retrieval performance under different levels of constraints, we considered 4 scenarios (Y0 to Y3). The scenario where all variables were optimized simultaneously is Y0. In Y0, to approximate total water content, we multiplied M_g by V_{veg} to evaluate the retrieval performance, omitting vegetation height and density as they were assumed constant. In addition to Y0, we introduced another scenario using a linearly-scaled LAI as input for vegetation volume (Y1). This approach aims to constrain the vegetation volume input by establishing a linear relationship between the measured LAI and the retrieved vegetation volume when both terms remain relatively stable during the growing season. This scenario helps evaluate the impact of vegetation volume changes on the dynamics of retrieved water content. Two additional scenarios were considered with vegetation volume fixed (Y2) and with canopy temperature fixed together (Y3). We then cross-compared the relationship between M_g and $\psi_{pd,l}$ across all scenarios to better understand the sensitivity of water content dynamics to changes in vegetation volume and temperature (which are tested across the scenarios).

https://doi.org/10.5194/egusphere-2026-4858
Preprint. Discussion started: 22 September 2026
© Author(s) 2026. CC BY 4.0 License.

2.8 Evaluation of VOD temperature dependency

To understand the physical basis for the additional information provided by dual-band observations, we evaluated the wavelength dependence of temperature sensitivity using both the electromagnetic model and GNSS observations. The full equations for parameterization of temperature effects in the electromagnetic model can be found in Ulaby and Long (2014). In the electromagnetic model tests, we ran several simulations with M_g values ranging from 0.4 to 0.7 g g^{-1} in increments of 0.1 g g^{-1} and temperature ranging from 10 to 40 °C in 1°C steps. The influence of V_{veg} on retrievals was not evaluated, as V_{veg} is assumed to not impact the dielectric loss of vegetation water as shown in Eq. (7).

3 Results

3.1 Retrieval improvement using dual-band synthetic data

We first quantified the theoretical information content of mono-band and dual-band VOD observations using the OSSE, where the true canopy state is known. The OSSE demonstrates that the additional information provided by a second frequency band improves retrieval performance, although the magnitude of this improvement depends strongly on VOD measurement precision.

For M_g, Bayesian inversion substantially reduces prior uncertainty under both mono-band and dual-band configurations (Figure 3a). Dual-band retrieval consistently outperforms mono-band retrieval, particularly when VOD observations are precise. For instance, the dual-band retrieval with a VOD error of 2% achieves a similar uncertainty reduction as mono-band retrieval with a VOD error of 0.5%. At a 4% VOD error, the M_g uncertainty reduction reaches 75%, corresponding to an absolute value of 0.042 g g^{-1}. This indicates that when the actual magnitude of M_g variation is within 0.042 g g^{-1}, even dual-band retrieval cannot fully distinguish this variation from its potential uncertainty. This threshold is particularly significant, as the 4% VOD measurement error aligns with our GNSS-based observations at the study site and the general M_g diurnal amplitude can reach 0.05 g g^{-1} (Humphrey & Frankenberg, 2023). Improving the precision of GNSS VOD estimates, such as through 3-hourly averaging while preserving the diurnal pattern, or deploying more sensors, could further improve retrieval performance.

For T_c, we found distinct differences between mono-band and dual-band retrievals, with dual-band retrievals consistently providing better results (Figure 3b). With high-precision VOD measurements (0.5% error), dual-band retrieval can reduce temperature uncertainty by up to 42% (i.e. from 4 K to 2.3 K). However, as the VOD measurement uncertainty increases, the reduction in temperature uncertainty becomes less pronounced. Mono-band retrieval, even with high precision VOD, fails to significantly reduce temperature uncertainty. Importantly, dual-band retrieval using two less precise VOD bands still outperforms mono-band retrieval when VOD measurements are highly precise, highlighting the greater benefit of incorporating an additional band over solely improving mono-band measurements precision for constraining T_c. However, this

https://doi.org/10.5194/egusphere-2026-4858
Preprint. Discussion started: 22 September 2026
© Author(s) 2026. CC BY 4.0 License.

benefit rapidly diminishes as observational uncertainty increases, indicating that the advantage of dual-band retrieval strongly depends on measurement precision.

The retrieval of V_{veg} follows a pattern similar to that of M_g, with dual-band retrieval providing greater uncertainty reduction as VOD measurement precision improves, achieving a maximum uncertainty reduction of ~85% (Figure 3c). The mono-band retrieval shows relatively stable performance across varying VOD uncertainty levels, while dual-band retrieval shows better performance with more precise VOD measurements. Similar to M_g, a 4% VOD measurement error indicates that only variations exceeding 27% of mean state can be effectively distinguished from uncertainty.

The diagonal elements in the averaging kernel matrices, which illustrate the sensitivity of retrieved variables to changes in the true state variables, support these findings. They show VOD observations provide strong constraints on M_g and V_{veg} but substantially weaker constraints on T_c under mono-band conditions (Figure S4). Reducing temperature uncertainty requires the addition of another closely-spaced band, while reducing uncertainty in water content can be achieved either by improving VOD precision or incorporating an additional closely-spaced band. Overall, the OSSE indicates that dual-band observations provide meaningful additional constraints primarily for canopy temperature. However, these theoretical benefits depend strongly on measurement precision, suggesting that retrieval performance under realistic GNSS observations may be considerably lower.

https://doi.org/10.5194/egusphere-2026-4858
Preprint. Discussion started: 22 September 2026
© Author(s) 2026. CC BY 4.0 License.

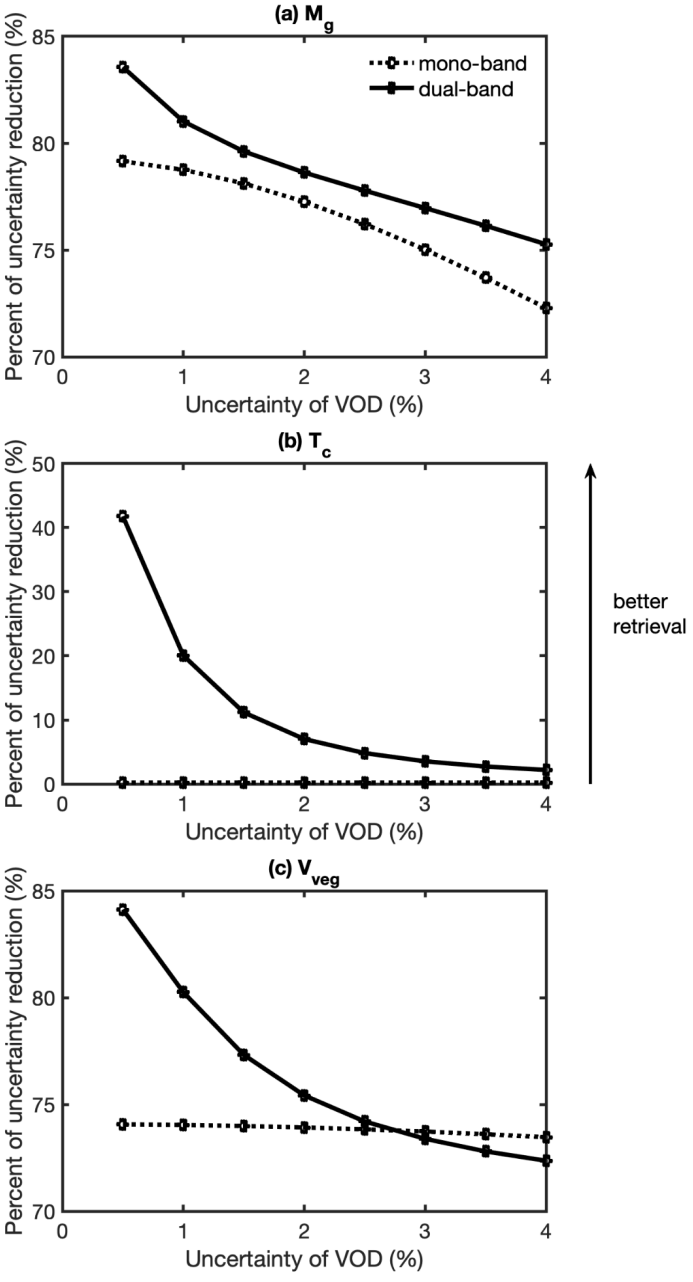

Figure 3. Performance of mono-band and dual-band retrievals in terms of uncertainty reduction for (a) M_g, (b) T_c, and c) V_{veg}. Results are based on testing eight VOD error levels ranging from 0.5% to 4% in 0.5% intervals.

365

https://doi.org/10.5194/egusphere-2026-4858
Preprint. Discussion started: 22 September 2026
© Author(s) 2026. CC BY 4.0 License.

3.2 Retrieval using GNSS VOD

3.2.1 Simultaneous retrieval

We next evaluated retrieval performance using GNSS observations at MOFLUX. Because VOD is expected to reflect vegetation water status, we first compared observed VOD and retrieved M_g against predawn leaf water potential during periods of stable canopy structure (LAI > 3). Observed VOD remained significantly correlated with $\psi_{pd,l}$ (Figure 4a,b), providing an appropriate benchmark for evaluating the retrieval. Note that the correlation between VOD and $\psi_{pd,l}$ is stronger for VOD at the L1 band compared to the L5 band. This difference may be attributed to the fact that the number of satellites tracking the L5 band is approximately half that of the L1 band, resulting in better-constrained data aggregation for the L1 band (Figure S1).

Despite this strong relationship between VOD and $\psi_{pd,l}$, simultaneous retrieval of M_g, T_c and V_{veg} (Scenario Y0) produces little correlation ($R^2 \approx 0$) between retrieved M_g and $\psi_{pd,l}$ (Figure 4c,d). This result is similar for both mono-band and dual-band retrievals, indicating that the additional information contained in the second frequency is insufficient to resolve the ambiguity among the three retrieved variables under realistic measurement uncertainty. Further examination of the retrieved variables provides insight into this behavior. We found that the retrieved T_c remained lower than the surface temperature inverted from outgoing long-wave radiation observations (Figure 4e, 4f), with no significant difference between mono-band and dual-band retrievals. Our retrieval analysis further showed that the estimated V_{veg} was unstable during this period, contrary to expectations based on a stable LAI (Figure 4g, 4h). The decrease in V_{veg} during the drydown period suggests that the drydown in late summer is being misinterpreted as a change in V_{veg} rather than changes in vegetation water content, which highlights the need for additional constraints on V_{veg} to achieve accurate M_g retrievals. These results indicate that simultaneous retrieval of M_g, T_c and V_{veg} remains strongly underconstrained under realistic GNSS observational uncertainty.

3.2.2 Sources of retrieval ambiguity

To identify which state variables are responsible for the retrieval ambiguity, we progressively constrained vegetation volume and canopy temperature. First, vegetation volume was constrained using a scaled LAI time series (Scenario Y1), assuming that vegetation structure varies slowly during the peak growing season. Under this constraint, the relationship between retrieved M_g and $\psi_{pd,l}$ improves, particularly under moderate water stress (Figure 5a,b). For example, the R^2 reached 0.35 when scaled LAI was used as input for V_{veg} when $\psi_{pd,l}$ is above -1.5 MPa. Similarly, assuming constant vegetation volume throughout the peak growing season (Scenario Y2) further improves the M_g–$\psi_{pd,l}$ relationship during less stressed periods (R^2>0.4, Figure 5c,d). These results indicate that the unconstrained retrieval tends to interpret drought-induced reductions in VOD as changes in vegetation volume rather than vegetation water content.

Because VOD responds to total canopy water rather than relative water content alone, we also evaluated the product $M_g \times V_{veg}$ as an approximation of total canopy water content. This metric exhibits a substantially stronger relationship with $\psi_{pd,l}$ than M_g alone (mono-band: R^2=0.35, dual-band: R^2=0.27, Figure 5e,f), suggesting that retrieving total canopy water

https://doi.org/10.5194/egusphere-2026-4858
Preprint. Discussion started: 22 September 2026
© Author(s) 2026. CC BY 4.0 License.

content may be more robust than independently separating M_g and V_{veg}. Therefore, to obtain reliable water content estimates from VOD, potential solutions include incorporating a reliable proxy for vegetation volume like leaf area index or estimating total water content without explicitly separating vegetation volume.

Even after forcing V_{veg} to remain constant during the peak growing season, the correlation between M_g and $\psi_{pd,l}$ did not reach the same level as the correlation between $\psi_{pd,l}$ and VOD (Figure 4a, 5c). Several data points at higher temperatures skewed this relationship. For instance, a VOD measured at 30°C and -0.5 MPa produced a similar M_g estimate (0.51 g g^{-1}) as a VOD measured at 15°C and -2.5 MPa (0.50 g g^{-1}) as shown in Figure 5c, indicating a slight over-sensitivity of VOD to temperature in the retrieval model. To further assess this, we held T_c constant and repeated the retrieval, finding that the correlation improved (Figure 5g,5h) and the temperature-induced bias in M_g was less than 10% of its magnitude - below the model's threshold for effective M_g retrieval (Figure 3a). This suggests that temperature effects on M_g cannot be reliably distinguished from the M_g uncertainty itself. Dual-band retrieval exhibited similar performance, likely because the relatively high VOD measurement uncertainty limits the additional benefit provided by dual-band observations (Figure 4, 5). Collectively, these diagnostic experiments demonstrate that the dominant limitation is not the absence of temperature information in dual-band VOD, but the inability to distinguish M_g, T_c and V_{veg} under realistic (~4%) observational uncertainty.

https://doi.org/10.5194/egusphere-2026-4858
Preprint. Discussion started: 22 September 2026
© Author(s) 2026. CC BY 4.0 License.

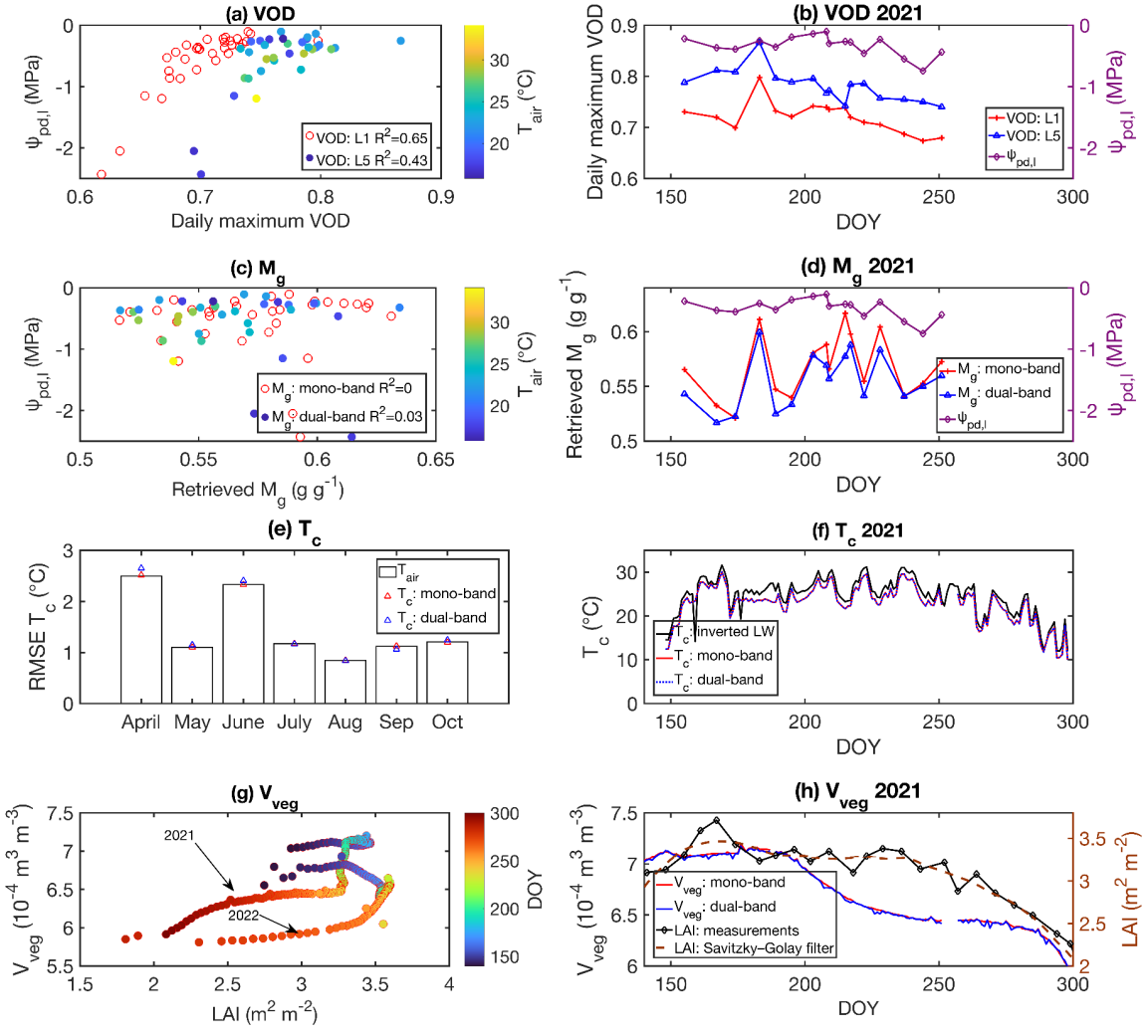

Figure 4. (a,b) GNSS VOD and retrieved components: (c,d) M_g, (e,f) T_c, (g,h) V_{veg}. In panel (c), M_g values from mono-band retrieval are represented by red circles, and dual-band retrievals are shown as dots, colored by the daily mean temperature. In panel (e), the RMSE between retrieved T_c and observed LST or RMSE between observed LST and T_{air} is calculated for each month. For simplicity, only data for the year 2021 is shown in panels (b,d,f,h), with the 2022 time series provided in Figure S5. The dynamic range of $\psi_{pd,l}$ is between -1 MPa and 0 for 2021. In panel (d), retrieved M_g is plotted on the left y-axis, and $\psi_{pd,l}$ on the right y-axis. In panel (h), vegetation volume is plotted on the left y-axis, with the LAI time series shown on the right y-axis.

https://doi.org/10.5194/egusphere-2026-4858
Preprint. Discussion started: 22 September 2026
© Author(s) 2026. CC BY 4.0 License.

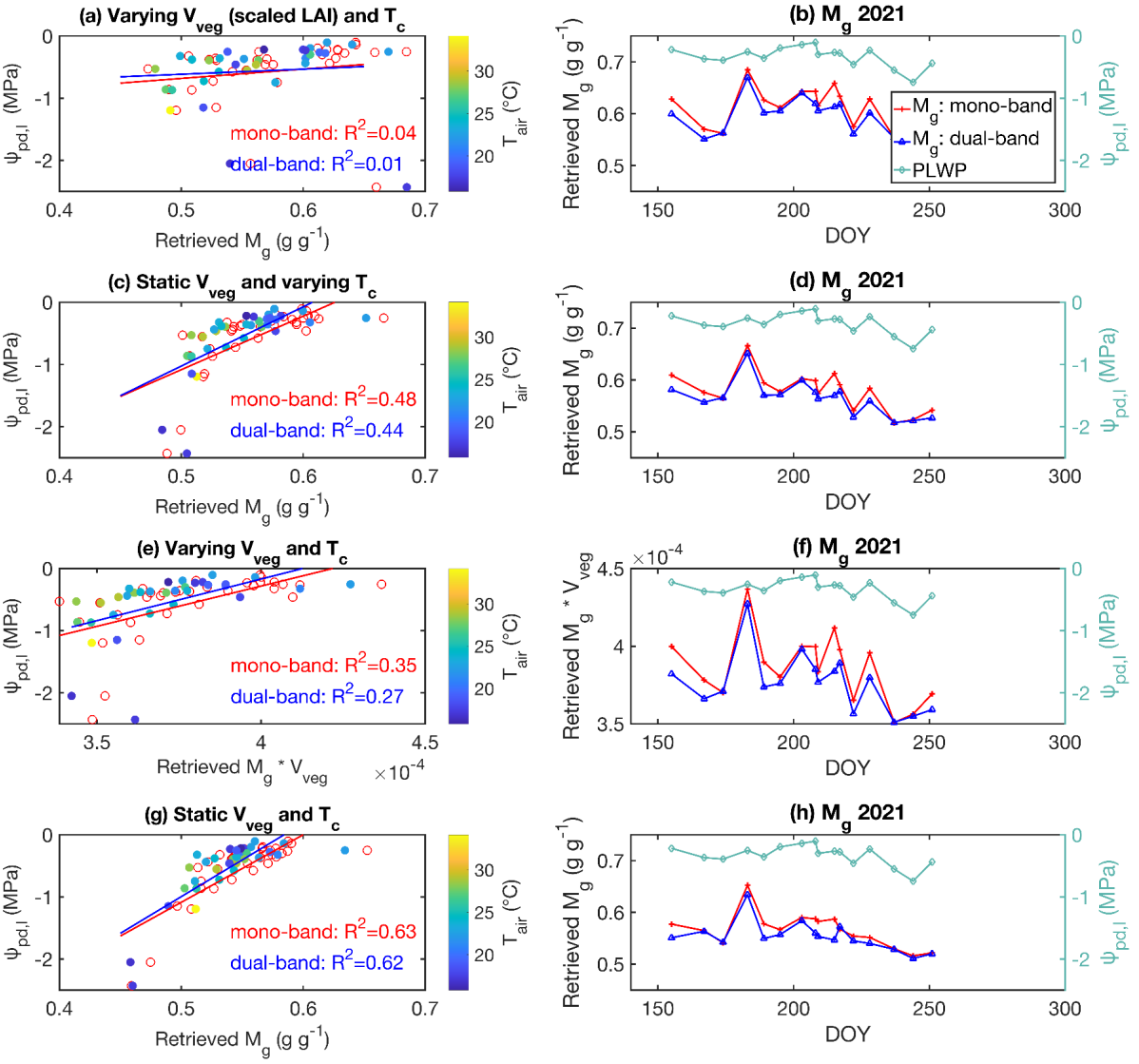

Figure 5. Relationship between retrieved M_g and $\psi_{pd,l}$. when (a,b) using V_{veg} scaled by LAI and varying T_c as input, (c,d) using static V_{veg} with varying T_c as input, (e,f) using varying V_{veg} and T_c as input but computing total water content, (g,h) using static V_{veg} and T_c as input. The time series for the year 2022 is provided in Figure S6. In panels (a,c,e,g), M_g values from mono-band retrieval are represented by red circles, and dual-band retrievals are shown as dots, colored by the daily mean temperature.

3.3 Temperature dependency across band frequencies

The OSSE (Section 3.1) suggests that dual-band observations primarily improve canopy temperature retrieval, whereas the retrieval experiments (Section 3.2) show that this theoretical advantage is largely lost under realistic GNSS

https://doi.org/10.5194/egusphere-2026-4858
Preprint. Discussion started: 22 September 2026
© Author(s) 2026. CC BY 4.0 License.

435 uncertainties. We therefore examine whether the expected wavelength-dependent temperature sensitivity can be detected directly in the GNSS observations. During the retrieval process, temperature information can only be extracted from dual-band VOD data (Figure 3b), indicating that it is the different temperature dependency across wavelengths that provides constraints on temperature magnitude. However, observational evidence of such temperature dependency across bands has been lacking, primarily due to the requirement for closely-spaced bands with similar penetration depths (such as L1 and L5 bands), which 440 are not available on current satellites. If bands are too far apart, VOD is also influenced by the different penetration depth, not only by the different sensitivity to temperature. Here, we provide observational evidence of different temperature dependencies across these two GNSS frequency bands.

The diurnal cycle provides an ideal test because vegetation volume remains nearly constant within a day, whereas 445 canopy water content and temperature vary strongly and often in opposite directions. Figure 6 shows the observed VOD diurnal cycle under low (surface soil moisture<30%) and high (surface soil moisture>=30%) soil moisture levels using GNSS measurements at the L1 and L5 bands. As shown in Yao et al. (2024), VOD at the L1 band exhibits a typical diurnal cycle, with lower values at noon and higher values before sunrise and after sunset, and a larger amplitude under greater stress. In contrast, the L5 VOD shows a much reduced diurnal amplitude. Similar to Humphrey & Frankenberg (2023), we infer that 450 temperature effects likely offset fluctuations in water content. By partitioning VOD variations into M_g and T_c, we found that the opposing diurnal cycles of temperature and water content, along with heightened temperature impacts, explain the flatter diurnal cycle of VOD at the L5 band (Figure S7). This temperature dependency in VOD across the two bands becomes more pronounced during heatwaves, with VOD at the L5 band even increasing around noon despite a potential sharp decline in water content (Figure S8). The distinct VOD diurnal cycle behaviors confirm the varying temperature dependencies across 455 bands.

We then evaluated the temperature dependency across bands in the electromagnetic model by comparing it with GNSS VOD measurements. Specifically, we analyzed the relationship between the L1/L5 ratio and temperature, as the L1/L5 ratio captures differences in temperature sensitivity between the two bands (Figure 7). Synthetic VOD from the 460 electromagnetic model shows that the L1/L5 ratio decreases as temperature increases (-0.22 to -0.33 %/°C), indicating that higher temperatures cause a greater VOD increase at the L5 band compared to the L1 band (Figure 7a). This behavior persists across different water content levels, with a slightly steeper negative slope in the L1/L5 ratio-to-temperature relationship under higher water content conditions (-0.33 %/°C when M_g reaches 0.7 g g^{-1}). GNSS measurements exhibit a similar behavior with a more negative slope (SMC>30%: -0.69 %/°C; SMC<=30%: -0.37%/°C) observed under wetter soil conditions when using 465 ordinary linear regression (Figure S9). However, when using weighted linear regression, the slope becomes more comparable between wetter and drier conditions (Figure 7b). The observed slope of the L1/L5 ratio to temperature is more negative (-0.4 ~ -0.42 %/°C) than that predicted by the electromagnetic model (-0.33 ~ -0.22 %/°C). Note that a scaling factor, obtained from dual-band retrieval (see Section 2.7.2 in Methods), was applied to the GNSS VOD at the L5 band to account for magnitude

https://doi.org/10.5194/egusphere-2026-4858
Preprint. Discussion started: 22 September 2026
© Author(s) 2026. CC BY 4.0 License.

mismatch with the electromagnetic model, which resulted in a more negative slope. The remaining differences may arise because the electromagnetic model assumes canopy temperature whereas the observations use air temperature as a proxy, and because within-canopy temperature heterogeneity is not represented in the current electromagnetic model. Despite these discrepancies, the GNSS VOD observations provide partial validation of the temperature dependency across bands as represented in the semi-empirical electromagnetic model. Combined with the OSSE and retrieval experiments, they indicate that dual-band observations do contain additional temperature information, but that the current GNSS measurement uncertainty is too large for this information to substantially improve retrieval performance.

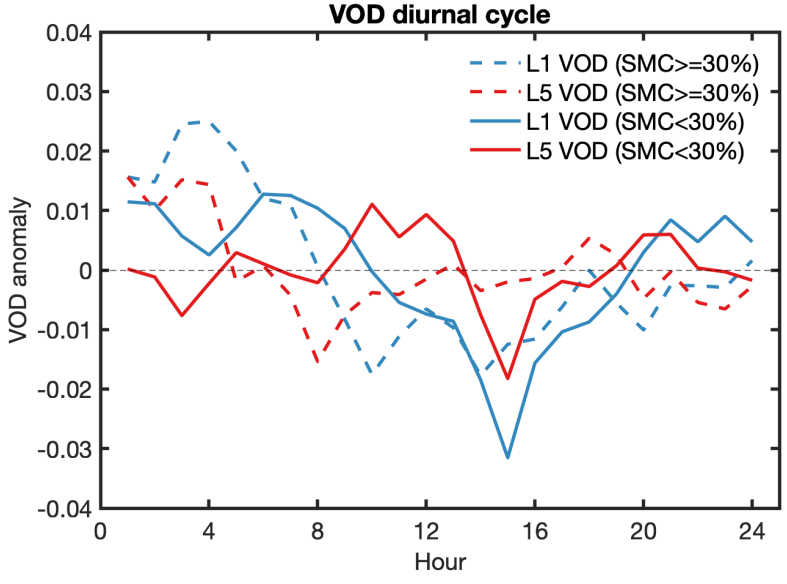

Figure 6. Average VOD diurnal cycle at different soil moisture content (SMC) levels. VOD anomalies are calculated by subtracting daily average values. Diurnal variations in VOD at the L1 band and L5 band are represented by solid and dashed lines, respectively.

https://doi.org/10.5194/egusphere-2026-4858
Preprint. Discussion started: 22 September 2026
© Author(s) 2026. CC BY 4.0 License.

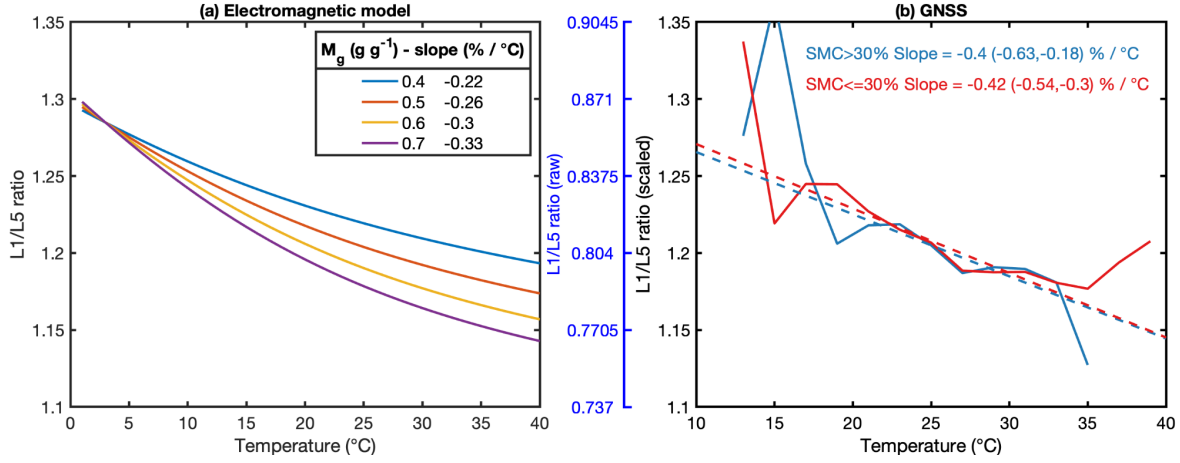

Figure 7. Relationship between the L1/L5 VOD ratio and temperature at varying canopy water content levels as derived from (a) the electromagnetic semi-empirical model and (b) GNSS observations. In panel (b), the data is categorized into two groups based on soil moisture content (SMC) levels. A scaling factor was applied to the VOD at the L5 band to account for the magnitude mismatch between the electromagnetic model and GNSS measurements at L5. This scaling factor was obtained from Bayesian inversion. To minimize the confounding effects of LAI changes, only data from periods with high LAI (LAI>=3.4) were included. A weighted linear regression was performed in panel (b), with the number of observations in each temperature bin serving as the weight.

4 Discussion

4.1 Underconstrained vegetation water content

Our study demonstrates that the primary limitation in retrieving vegetation water content from VOD is not the inability of microwave observations to sense vegetation water, but the ambiguity introduced by simultaneously retrieving M_g, V_{veg}, and T_c. Although Bayesian inversion successfully reduced uncertainty in the OSSE, retrieval performance deteriorated when applied to real GNSS observations because VOD variations could not be uniquely attributed to these three state variables. The strongest evidence comes from the substantial improvement in M_g retrieval after constraining vegetation volume using either scaled LAI or a constant V_{veg}. These results indicate that the inversion preferentially attributes day-to-day VOD variations to changes in vegetation volume rather than vegetation water content. This finding agrees well with Chaparro et al. (2024), who also reported that temporally averaged vegetation volume produces more realistic water-content retrievals than allowing vegetation volume to vary freely. Estimating relative water content from VOD often implicitly assumes that vegetation structure remains nearly constant over short time scales (Hellwig et al., 2023). While oversensitivity to V_{veg} may not significantly impact the diurnal cycle, it can affect day-to-day comparisons of water content. Our results therefore suggest that future VOD retrieval algorithms should prioritize independent structural constraints, such as LAI or other canopy structural observations, rather than relying solely on microwave observations to retrieve both structure and physiology simultaneously.

https://doi.org/10.5194/egusphere-2026-4858
Preprint. Discussion started: 22 September 2026
© Author(s) 2026. CC BY 4.0 License.

Another important source of uncertainty arises from the mismatch between the quantities sensed by microwave observations and those measured in the field. The overall relationship between VOD and leaf water potential incorporates both the pressure-volume curve and water content-dielectric constant relationships. Predawn leaf water potential primarily reflects leaf hydraulic status, whereas L-band VOD integrates water stored throughout the canopy, including stems and branches. Consequently, retrieved M_g is not expected to correlate perfectly with $\psi_{pd,l}$, even if the retrieval itself were perfect. This interpretation is consistent with Holtzman et al. (2021), who reported stronger relationships between VOD and leaf water potential than between dielectric properties and leaf water potential. Shorter wavelengths, such as X-band and Ku-band VOD, might provide better constraints on canopy moisture due to their greater sensitivity to leaf-level water content (Chaparro et al., 2024). The relationship between water potential, canopy water content, and VOD is further complicated by nonlinear pressure-volume relationships, particularly under severe drought. Better field experiments simultaneously measuring leaf water potential, whole-canopy water content, and microwave observations will therefore be essential for establishing step-by-step quantitative relationships across these variables.

In addition to the substantial influence of dynamic V_{veg} on the correlation between retrieved M_g and $\psi_{pd,l}$, discrepancies where similar retrieved M_g values correspond to markedly different $\psi_{pd,l}$ readings could also arise from the cross-correlation between temperature and water potential. Independent dielectric models and laboratory measurements consistently support the positive temperature dependence implemented in our electromagnetic model (Schwank et al., 2021; Zhao et al., 2024; Romanov and Ulanov, 2019; Romanov, 2022), suggesting that model structural errors are unlikely to explain the observed retrieval ambiguity. This finding underscores the need for caution when interpreting the partitioning of the VOD diurnal cycle into temperature and water content variations, as temperature-related confounding effects are more pronounced on a diurnal scale. Since interactions between temperature, water content, water salinity, and wavelength are encoded empirically, more experimental studies are necessary to properly diagnose temperature's contributions and to develop a more accurate representation of the water content diurnal cycle. This is crucial for assessing water stress through the diurnal hysteresis effect (Lin et al., 2019; Nelson et al., 2018; Zhang et al., 2014).

4.2 Limited improvement with dual-band retrieval

By determining water content, temperature, and vegetation volume from VOD data streams, our work presents the first direct comparison of the information provided by mono-band and dual-band VOD measurements for interpreting VOD dynamics. Using a synthetic data experiment, we found that dual-band VOD measurements provide greater accuracy especially for temperature, reducing temperature uncertainty by up to 42% in the best-case scenarios and by about 12% on average. In contrast, even highly precise mono-band measurements are insufficient for effectively constraining temperature changes. This suggests that the additional information gain for temperature mainly arises from differences in temperature sensitivity across the two bands. To achieve more reliable temperature estimates, either high-precision VOD measurements at another closely-

https://doi.org/10.5194/egusphere-2026-4858
Preprint. Discussion started: 22 September 2026
© Author(s) 2026. CC BY 4.0 License.

spaced band or greater temperature sensitivity between bands is necessary, as temperature induced VOD changes are less than 1% per 1 °C change (Figure 1). Specifically, temperature-induced VOD variations must exceed their internal uncertainty levels. Otherwise, the current retrieval system will be unable to correctly attribute VOD variations to temperature changes. We further explored temperature sensitivity across different bands (Figure S10) and found that two less closely-spaced bands offer higher temperature sensitivity. However, we acknowledge that the benefits of the second closely-spaced band emerge only when VOD uncertainty is relatively low. When VOD uncertainty reaches 4% as observed in our GNSS VOD measurements, the performance difference between mono-band and dual-band retrievals become negligible (Figure 3b).

Our analysis further indicates that improving measurement precision is at least as important as increasing the number of observation frequencies. In the OSSE, dual-band retrieval with 2% VOD uncertainty performs similarly to mono-band retrieval with 0.5% uncertainty, illustrating that the benefit of additional frequencies strongly depends on measurement quality. Moreover, our experiments suggest that the usefulness of additional observations depends not only on their precision but also on the independence of their error sources. When both bands share similar measurement uncertainties, the additional information remains limited because the errors are highly correlated. Conversely, combining observations with independent uncertainties offers greater potential for uncertainty reduction than simply adding another measurement with similar characteristics. This finding suggests that future microwave missions should prioritize both lower measurement uncertainty and independent observational constraints, rather than simply increasing the number of frequencies.

4.3 Implications for interpreting VOD dynamics

Although our study focuses on retrieval methodology, the results also have broader implications for interpreting microwave observations of vegetation dynamics. Several recent studies have reported unexpected VOD behavior during drought, including positive VOD anomalies despite declining soil moisture and vegetation greenness (Buitink et al., 2020; Entekhabi, 2023; Konkathi and Karthikeyan, 2024). Similar discrepancies have also been observed in diurnal VOD cycles derived from SMOS, where daytime VOD occasionally exceeds nighttime values (Dou et al., 2023). These behaviors have been attributed to a variety of mechanisms, including measurement artifacts, dew formation, xylem refilling, and changes in plant hydraulics.

Our analysis suggests that temperature-dependent dielectric properties may provide an additional explanation for these observations. Because increasing temperature partially offsets the reduction in VOD caused by declining vegetation water content, VOD anomalies during periods of water stress may not directly reflect changes in plant water status alone. Temperature effects are expected to be particularly important when interpreting diurnal VOD dynamics because canopy temperature and vegetation water content vary simultaneously but in opposite directions. Future studies should therefore carefully account for temperature before attributing VOD anomalies solely to changes in vegetation water status. One practical solution is to report either total canopy water content or VOD standardized to a reference temperature (e.g., 25 °C), thereby minimizing temperature-induced variability. Although the standardization coefficient depends on both temperature and

https://doi.org/10.5194/egusphere-2026-4858
Preprint. Discussion started: 22 September 2026
© Author(s) 2026. CC BY 4.0 License.

vegetation water content (Figure S11), our results indicate that temperature alone explains most of its variation. Temperature normalization therefore offers a simple approach to reduce one of the major confounding factors in interpreting VOD dynamics across regions and environmental conditions.

4.4 Limitations and future perspectives

Several assumptions and simplifications in our methodology should be acknowledged. First, we applied a scaling factor to address the observed discrepancy where GNSS VOD at the L5 band was higher than at the L1 band, which is contrary to the estimations from the electromagnetic model. When we plotted the VOD distribution across hemispheric space, we found that this bias was more pronounced in clear-sky areas with very low VOD magnitudes (Figure S12, S13). After filtering out these lower VOD values in clear-sky areas, the aggregated VOD at the L5 band decreased, while VOD at the L1 band increased. Although this filtering brought the VOD ratio between the two bands closer to the electromagnetic model's estimates, a non-negligible difference remained. This discrepancy may arise because the current model assumes homogeneous canopy properties and neglects wavelength-dependent scattering from woody tissues. Future electromagnetic models that explicitly represent branches and multiple scattering processes should help improve multi-frequency retrievals. Additionally, in GNSS systems, the difference between the L1 and L5 bands is influenced not only by wavelength but also by differences in power and signal characteristics dependent on the transmitting satellites, factors that are not accounted for in the current electromagnetic models.

Second, GNSS VOD uncertainty was estimated from nighttime observations under the assumption that canopy water status remains relatively stable during this period. Processes such as nocturnal rehydration or dew formation may violate this assumption, resulting in conservative estimates of observational uncertainty. Increasing the number of GNSS receivers beneath the canopy or improving temporal averaging strategies should help reduce measurement uncertainty and better exploit the additional information available from multiple frequencies.

Third, canopy temperature priors were approximated using air temperature observations. While appropriate for the well-instrumented MOFLUX site, this assumption may not hold for broader operational applications where canopy temperature observations are unavailable. When only a loose prior for canopy temperature is available (e.g., a prior value of 20 °C with an associated uncertainty of ±20 °C), the retrieval can reduce temperature uncertainty to no better than ±4 °C. Developing retrieval frameworks that rely on weaker prior information or complementary thermal infrared observations will therefore be important for future applications.

Beyond these methodological limitations, our results also point toward several opportunities for future observing systems. Improving retrieval performance will require not only additional observation frequencies, but also substantially lower measurement uncertainty and complementary observations of canopy structure. For example, LAI data might effectively capture canopy development dynamics during the growing season, thereby helping to reduce the equifinality issue. This combined approach can help mitigate the challenges of using VOD alone, providing a more comprehensive understanding of water dynamics across different ecosystems.

https://doi.org/10.5194/egusphere-2026-4858
Preprint. Discussion started: 22 September 2026
© Author(s) 2026. CC BY 4.0 License.

Future satellite missions provide exciting opportunities to test these ideas. Missions such as NISAR and ROSE-L will extend L-band observations toward longer wavelengths (1.25 GHz), while ESA's CIMR mission will provide coordinated observations across multiple microwave frequencies (Vanin et al., 2020). These observations, particularly when combined across platforms with partially independent error sources, may allow future retrieval systems to exploit the wavelength-dependent temperature sensitivity demonstrated here. However, challenges associated with data assimilation from multiple satellites still remain, as co-locating measurements from sensors with different temporal and spatial resolutions onto a common grid and time requires careful postprocessing. Additionally, low Earth orbit satellites generally have minimal temporal overlap, further complicating synergistic use. Nevertheless, this capability will likely offer valuable insights into validating temperature dependencies and disentangling temperature-related confounding effects at large spatial scales. By refining VOD interpretations under diverse environmental conditions, these advancements hold the potential to enable more accurate and robust assessments of vegetation moisture dynamics.

Code availability:

The code for reproducing all results in this study has been archived at https://doi.org/10.5281/zenodo.21917819 (Yao and Humphrey, 2026).

Data availability:

Ecosystem flux data for MOFLUX is available at Wood and Gu (2022). Predawn leaf water potential measurement is available at Pallardy et al. (2018). Other auxiliary data can be found at Yao & Humphrey (2026).

Author contributions

YY and CF designed the study. YY conducted the analysis and wrote the initial draft. All authors contributed to the interpretation of the results and writing the manuscript.

Competing interests

The authors declare that there is no conflict of interest regarding the publication of this article.

https://doi.org/10.5194/egusphere-2026-4858
Preprint. Discussion started: 22 September 2026
© Author(s) 2026. CC BY 4.0 License.

Financial support

This work was supported by NASA Carbon Cycle Science Grant 80NSSC21K1712. AGK was also supported by the Alfred P. Sloan Foundation and NASA Soil Moisture Active Passive Grant 80NSSC25K7055. V. Humphrey was supported by the Swiss National Science Foundation (grant no. P4P4P2_194464).

References

Buitink, J., Swank, A.M., van der Ploeg, M., Smith, N.E., Benninga, H.-J.F., van der Bolt, F., Carranza, C.D.U., Koren, G., van der Velde, R., Teuling, A.J.: Anatomy of the 2018 agricultural drought in the Netherlands using in situ soil moisture and satellite vegetation indices. Hydrol. Earth Syst. Sci. 24, 6021–6031. https://doi.org/10.5194/hess-24-6021-2020, 2020.

Chaparro, D., Jagdhuber, T., Piles, M., Jonard, F., Fluhrer, A., Vall-llossera, M., Camps, A., López-Martínez, C., Fernández-Morán, R., Baur, M., Feldman, A.F., Fink, A., Entekhabi, D.: Vegetation moisture estimation in the Western United States using radiometer-radar-lidar synergy. Remote Sens. Environ. 303, 113993. https://doi.org/10.1016/j.rse.2024.113993, 2024.

Dou, Y., Tian, F., Wigneron, J.-P., Tagesson, T., Du, J., Brandt, M., Liu, Y., Zou, L., Kimball, J.S., Fensholt, R.: Reliability of using vegetation optical depth for estimating decadal and interannual carbon dynamics. Remote Sens. Environ. 285, 113390. https://doi.org/10.1016/j.rse.2022.113390, 2023.

Dutta, D., Schimel, D.S., Sun, Y., van der Tol, C., Frankenberg, C.: Optimal inverse estimation of ecosystem parameters from observations of carbon and energy fluxes. Biogeosciences 16, 77–103. https://doi.org/10.5194/bg-16-77-2019, 2019.

Entekhabi, D.: Propagation in the drought cascade: Observational analysis over the continental US. Water Resour. Res. 59. https://doi.org/10.1029/2022wr032608, 2023.

Fan, L., Wigneron, J.-P., Ciais, P., Chave, J., Brandt, M., Fensholt, R., Saatchi, S.S., Bastos, A., Al-Yaari, A., Hufkens, K., Qin, Y., Xiao, X., Chen, C., Myneni, R.B., Fernandez-Moran, R., Mialon, A., Rodriguez-Fernandez, N.J., Kerr, Y., Tian, F., Peñuelas, J.: Satellite-observed pantropical carbon dynamics. Nat. Plants 5, 944–951. https://doi.org/10.1038/s41477-019-0478-9, 2019.

Fan, L., Wigneron, J.-P., Ciais, P., Chave, J., Brandt, M., Sitch, S., Yue, C., Bastos, A., Li, X., Qin, Y., Yuan, W., Schepaschenko, D., Mukhortova, L., Li, X., Liu, X., Wang, M., Frappart, F., Xiao, X., Chen, J., Ma, M., Wen, J., Chen, X., Yang, H., van Wees, D., Fensholt, R.: Siberian carbon sink reduced by forest disturbances. Nat. Geosci. 16, 56–62. https://doi.org/10.1038/s41561-022-01087-x, 2023.

Forkel, M., Schmidt, L., Zotta, R.-M., Dorigo, W., Yebra, M.: Estimating leaf moisture content at global scale from passive microwave satellite observations of vegetation optical depth. Hydrol. Earth Syst. Sci. 27, 39–68. https://doi.org/10.5194/hess-27-39-2023, 2023.

Gu, L., Pallardy, S.G., Hosman, K.P., Sun, Y.: Impacts of precipitation variability on plant species and community water stress in a temperate deciduous forest in the central US. Agric. For. Meteorol. 217, 120–136. https://doi.org/10.1016/j.agrformet.2015.11.014, 2016.

https://doi.org/10.5194/egusphere-2026-4858
Preprint. Discussion started: 22 September 2026
© Author(s) 2026. CC BY 4.0 License.

Gu, L., Pallardy, S.G., Hosman, K.P., Sun, Y.: Drought-influenced mortality of tree species with different predawn leaf water dynamics in a decade-long study of a central US forest. Biogeosciences 12, 2831–2845. https://doi.org/10.5194/bg-12-2831-2015, 2015.

Hellwig, F.M., Jagdhuber, T., Fluhrer, A., Dubois, C., Chaparro, D., Schellenberg, K., Piles, M., Schmullius, C., Entekhabi, D.: Multi-frequency radiometry for multi-year monitoring of relative water content in A temperate forest, in: IGARSS 2023 - 2023 IEEE International Geoscience and Remote Sensing Symposium. Presented at the IGARSS 2023 - 2023 IEEE International Geoscience and Remote Sensing Symposium, IEEE. https://doi.org/10.1109/igarss52108.2023.10281760, 2023.

Holtzman, N., Wang, Y., Wood, J.D., Frankenberg, C., Konings, A.G.: Constraining plant hydraulics with microwave radiometry in a land surface model: Impacts of temporal resolution. Water Resour. Res. 59. https://doi.org/10.1029/2023wr035481, 2023.

Humphrey, V., & Frankenberg, C.: Continuous ground monitoring of vegetation optical depth and water content with GPS signals. Biogeosciences 20, 1789–1811. https://doi.org/10.5194/bg-20-1789-2023, 2023.

Jackson, T.J., & Schmugge, T.J.: Vegetation effects on the microwave emission of soils. Remote Sens. Environ. 36, 203–212. https://doi.org/10.1016/0034-4257(91)90057-D, 1991.

Jagdhuber, T., Schmidt, A.-S., Fluhrer, A., Chaparro, D., Jonard, F., Piles, M., Holtzman, N., Konings, A.G., Feldman, A.F., Baur, M.J., Steele-Dunne, S., Schellenberg, K., Kunstmann, H.: Estimation of forest water potential from ground-based L-band radiometry. IEEE J. Sel. Top. Appl. Earth Obs. Remote Sens. 18, 5509–5522. doi: 10.1109/JSTARS.2025.3533567, 2025.

Konings, A.G., Holtzman, N.M., Rao, K., Xu, L., Saatchi, S.S.: Interannual variations of vegetation optical depth are due to both water stress and biomass changes. Geophys. Res. Lett. 48. https://doi.org/10.1029/2021gl095267, 2021a.

Konings, A.G., Rao, K., Steele-Dunne, S.C.: Macro to micro: microwave remote sensing of plant water content for physiology and ecology. New Phytol. 223, 1166–1172. https://doi.org/10.1111/nph.15808, 2019.

Konings, A.G., Saatchi, S.S., Frankenberg, C., Keller, M., Leshyk, V., Anderegg, W.R.L., Humphrey, V., Matheny, A.M., Trugman, A., Sack, L., Agee, E., Barnes, M.L., Binks, O., Cawse-Nicholson, K., Christoffersen, B.O., Entekhabi, D., Gentine, P., Holtzman, N.M., Katul, G.G., Liu, Y., Longo, M., Martinez-Vilalta, J., McDowell, N., Meir, P., Mencuccini, M., Mrad, A., Novick, K.A., Oliveira, R.S., Siqueira, P., Steele-Dunne, S.C., Thompson, D.R., Wang, Y., Wehr, R., Wood, J.D., Xu, X., Zuidema, P.A.: Detecting forest response to droughts with global observations of vegetation water content. Glob. Chang. Biol. 27, 6005–6024. https://doi.org/10.1111/gcb.15872, 2021b.

Konkathi, P., & Karthikeyan, L.: Utility of L-band and X-band vegetation optical depth to examine vegetation response to soil moisture droughts in South Asia. Remote Sens. Environ. 301, 113933. https://doi.org/10.1016/j.rse.2023.113933, 2024.

Kumar, S.V., Holmes, T., Andela, N., Dharssi, I., Vinodkumar, Hain, C., Peters-Lidard, C., Mahanama, S.P., Arsenault, K.R., Nie, W., Getirana, A.: The 2019–2020 Australian drought and bushfires altered the partitioning of hydrological fluxes. Geophys. Res. Lett. 48. https://doi.org/10.1029/2020gl091411, 2021.

Lagarias, J.C., Reeds, J.A., Wright, M.H., Wright, P.E.: Convergence properties of the Nelder--mead simplex method in low dimensions. SIAM J. Optim. 9, 112–147. https://doi.org/10.1137/S1052623496303470, 1998.

https://doi.org/10.5194/egusphere-2026-4858
Preprint. Discussion started: 22 September 2026
© Author(s) 2026. CC BY 4.0 License.

Levenberg, K.: A method for the solution of certain non – linear problems in least squares. Quarterly of Applied Mathematics 2, 164–168. https://www.jstor.org/stable/43633451, 1944.

Lin, C., Gentine, P., Frankenberg, C., Zhou, S., Kennedy, D., Li, X.: Evaluation and mechanism exploration of the diurnal hysteresis of ecosystem fluxes. Agric. For. Meteorol. 278, 107642. https://doi.org/10.1016/j.agrformet.2019.107642, 2019.

Liu, K., Wang, Y., Magney, T.S., Frankenberg, C.: Non-steady-state stomatal conductance modeling and its implications: from leaf to ecosystem. Biogeosciences 21, 1501–1516. https://doi.org/10.5194/bg-21-1501-2024, 2024.

Liu, Y., Holtzman, N.M., Konings, A.G.: Global ecosystem-scale plant hydraulic traits retrieved using model–data fusion. Hydrol. Earth Syst. Sci. 25, 2399–2417. https://doi.org/10.5194/hess-25-2399-2021, 2021.

Marquardt, D.: An algorithm for least-squares estimation of nonlinear parameters. Journal of The Society for Industrial and Applied Mathematics 11, 431–441. https://www.jstor.org/stable/2098941, 1963.

Momen, M., Wood, J.D., Novick, K.A., Pangle, R., Pockman, W.T., McDowell, N.G., Konings, A.G.: Interacting Effects of Leaf Water Potential and Biomass on Vegetation Optical Depth. Journal of Geophysical Research: Biogeosciences 122, 3031–3046. https://doi.org/10.1002/2017JG004145, 2017.

Nelson, J.A., Carvalhais, N., Migliavacca, M., Reichstein, M., Jung, M.: Water-stress-induced breakdown of carbon–water relations: indicators from diurnal FLUXNET patterns. Biogeosciences 15, 2433–2447. https://doi.org/10.5194/bg-15-2433-2018, 2018.

Novick, K.A., Ficklin, D.L., Grossiord, C., Konings, A.G., Martínez-Vilalta, J., Sadok, W., Trugman, A.T., Williams, A.P., Wright, A.J., Abatzoglou, J.T., Dannenberg, M.P., Gentine, P., Guan, K., Johnston, M.R., Lowman, L.E.L., Moore, D.J.P., McDowell, N.G.: The impacts of rising vapour pressure deficit in natural and managed ecosystems. Plant Cell Environ. 47, 3561–3589. https://doi.org/10.1111/pce.14846, 2024.

Pallardy, S. G., Gu, L., Wood, J. D., Hosman, K. P., & Sun, Y.: Predawn leaf water potential of oak-hickory forest at Missouri Ozark (MOFLUX) site: 2004–2021 [Dataset]. Oak Ridge National Laboratory, TES SFA, U.S. Department of Energy. https://doi.org/10.3334/CDIAC/ornlsfa.004, 2018.

Piao, S., Zhang, X., Chen, A., Liu, Q., Lian, X., Wang, X., Peng, S., Wu, X.: The impacts of climate extremes on the terrestrial carbon cycle: A review. Sci. China Earth Sci. 62, 1551–1563. https://doi.org/10.1007/s11430-018-9363-5, 2019.

Rao, K., Anderegg, W.R.L., Sala, A., Martínez-Vilalta, J., Konings, A.G.: Satellite-based vegetation optical depth as an indicator of drought-driven tree mortality. Remote Sens. Environ. 227, 125–136. https://doi.org/10.1016/j.rse.2019.03.026, 2019.

Rao, K., Williams, A.P., Diffenbaugh, N.S., Yebra, M., Konings, A.G.: Plant-water sensitivity regulates wildfire vulnerability. Nat. Ecol. Evol. 6, 332–339. https://doi.org/10.1038/s41559-021-01654-2, 2022.

Reichstein, M., Bahn, M., Ciais, P., Frank, D., Mahecha, M.D., Seneviratne, S.I., Zscheischler, J., Beer, C., Buchmann, N., Frank, D.C., Papale, D., Rammig, A., Smith, P., Thonicke, K., van der Velde, M., Vicca, S., Walz, A., Wattenbach, M.: Climate extremes and the carbon cycle. Nature 500, 287–295. https://doi.org/10.1038/nature12350, 2013.

https://doi.org/10.5194/egusphere-2026-4858
Preprint. Discussion started: 22 September 2026
© Author(s) 2026. CC BY 4.0 License.

Rodgers, C.D.: Inverse methods for atmospheric sounding: Theory and practice: Theory and practice, Series On Atmospheric, Oceanic And Planetary Physics. World Scientific Publishing, Singapore, Singapore. https://doi.org/10.1142/3171, 2000.

Romanov, A.N.: Some behavior features of dielectric properties of water in birch wood at a frequency of 1.41 GHz. IEEE Trans. Geosci. Remote Sens. 60, 1–8. doi: 10.1109/TGRS.2022.3157642, 2022.

Romanov, A.N., Ulanov, P.N.: Seasonal differences in dielectric properties of dwarf woody tundra vegetation in a microwave range. IEEE Trans. Geosci. Remote Sens. 57, 3119–3125. doi: 10.1109/TGRS.2018.2881048. 2019.

Roy, A., Toose, P., Mavrovic, A., Pappas, C., Royer, A., Derksen, C., Berg, A., Rowlandson, T., El-Amine, M., Barr, A., Black, A., Langlois, A., Sonnentag, O.: L-Band response to freeze/thaw in a boreal forest stand from ground- and tower-based radiometer observations. Remote Sens. Environ. 237, 111542. https://doi.org/10.1016/j.rse.2019.111542, 2020.

Schwank, M., Kontu, A., Mialon, A., Naderpour, R., Houtz, D., Lemmetyinen, J., Rautiainen, K., Li, Q., Richaume, P., Kerr, Y., Mätzler, C.: Temperature effects on L-band vegetation optical depth of a boreal forest. Remote Sens. Environ. 263, 112542. https://doi.org/10.1016/j.rse.2021.112542, 2021.

Still, C.J., Page, G., Rastogi, B., Griffith, D.M., Aubrecht, D.M., Kim, Y., Burns, S.P., Hanson, C.V., Kwon, H., Hawkins, L., Meinzer, F.C., Sevanto, S., Roberts, D., Goulden, M., Pau, S., Detto, M., Helliker, B., Richardson, A.D.: No evidence of canopy-scale leaf thermoregulation to cool leaves below air temperature across a range of forest ecosystems. Proc. Natl. Acad. Sci. U. S. A. 119, e2205682119. https://doi.org/10.1073/pnas.2205682119, 2022.

Tian, F., Wigneron, J.-P., Ciais, P., Chave, J., Ogée, J., Peñuelas, J., Ræbild, A., Domec, J.-C., Tong, X., Brandt, M., Mialon, A., Rodriguez-Fernandez, N., Tagesson, T., Al-Yaari, A., Kerr, Y., Chen, C., Myneni, R.B., Zhang, W., Ardö, J., Fensholt, R.: Coupling of ecosystem-scale plant water storage and leaf phenology observed by satellite. Nat. Ecol. Evol. 2, 1428–1435. https://doi.org/10.1038/s41559-018-0630-3, 2018.

Ulaby, F. T., & El-Rayes, M.: Microwave dielectric spectrum of vegetation - Part II: Dual-dispersion model. IEEE Transactions on Geoscience and Remote Sensing GE, 25(5), 550–557. https://doi.org/10.1109/tgrs.1987.289833, 1987.

Ulaby, F. T., & Long, D. G.: Microwave radar and radiometric remote sensing (Vol. 2014). University of Michigan Press. https://doi.org/10.3998/0472119356, 2014.

Vanin, F., Laberinti, P., Donlon, C., Fiorelli, B., Barat, I., Sole, M.P., Palladino, M., Eggers, P., Rudolph, T., Galeazzi, C.: Copernicus imaging microwave radiometer (CIMR): System aspects and technological challenges, in: IGARSS 2020 - 2020 IEEE International Geoscience and Remote Sensing Symposium. Presented at the IGARSS 2020 - 2020 IEEE International Geoscience and Remote Sensing Symposium, IEEE, pp. 6535–6538. doi: 10.1109/IGARSS39084.2020.9324259. 2020.

Wigneron, J.-P., Ciais, P., Li, X., Brandt, M., Canadell, J.G., Tian, F., Wang, H., Bastos, A., Fan, L., Gatica, G., Kashyap, R., Liu, X., Sitch, S., Tao, S., Xiao, X., Yang, H., Espinoza Villar, J.C., Frappart, F., Li, W., Qin, Y., De Truchis, A., Fensholt, R.: Global carbon balance of the forest: satellite-based L-VOD results over the last decade. Front. Remote Sens. 5. https://doi.org/10.3389/frsen.2024.1338618, 2024.

Wood, J., & Gu, L.: AmeriFlux FLUXNET-1F US-MOz Missouri Ozark site [Dataset]. AMF. https://doi.org/10.17190/AMF/1854370, 2022.

https://doi.org/10.5194/egusphere-2026-4858
Preprint. Discussion started: 22 September 2026
© Author(s) 2026. CC BY 4.0 License.

Wood, J.D., Gu, L., Hanson, P.J., Frankenberg, C., Sack, L.: The ecosystem wilting point defines drought response and recovery of a Quercus-Carya forest. Glob. Chang. Biol. 29, 2015–2029. https://doi.org/10.1111/gcb.16582, 2023.

Wood, J., Widmer, B., Anderson, D., Pallardy, S., Gu, L., Hosman, K.: Leaf-area index of Oak-Hickory Forest at Missouri Ozark (MOFLUX) site: 2007–2022. https://doi.org/10.25581/ORNLSFA.028/1906782, 2022.

Xiao, C., Zaehle, S., Yang, H., Wigneron, J.-P., Schmullius, C., Bastos, A.: Land cover and management effects on ecosystem resistance to drought stress. Earth Syst. Dynam. 14, 1211–1237. https://doi.org/10.5194/esd-14-1211-2023, 2023.

Yang, H., Ciais, P., Frappart, F., Li, X., Brandt, M., Fensholt, R., Fan, L., Saatchi, S., Besnard, S., Deng, Z., Bowring, S., Wigneron, J.-P.: Global increase in biomass carbon stock dominated by growth of northern young forests over past decade. Nat. Geosci. 16, 886–892. https://doi.org/10.1038/s41561-023-01274-4, 2023.

Yao, Y., Humphrey, V., Konings, A.G., Wang, Y., Yin, Y., Holtzman, N., Wood, J.D., Bar-On, Y., Frankenberg, C.: Investigating diurnal and seasonal cycles of vegetation optical depth retrieved from GNSS signals in a broadleaf forest. Geophys. Res. Lett. 51. https://doi.org/10.1029/2023gl107121, 2024.

Yao, Y., Humphrey, V.: Dual-band information helps constrain canopy water content and temperature retrievals from vegetation optical depth. Zenodo [code], https://doi.org/10.5281/zenodo.21917819, 2026.

Zhang, Q., Manzoni, S., Katul, G., Porporato, A., Yang, D.: The hysteretic evapotranspiration-Vapor pressure deficit relation: ET-VPD hysteresis. J. Geophys. Res. Biogeosci. 119, 125–140. https://doi.org/10.1002/2013JG002484, 2014.

Zhao, M., Humphrey, V., Feldman, A.F., Konings, A.G.: Temperature is likely an important omission in interpreting vegetation optical depth. Geophys. Res. Lett. 51. https://doi.org/10.1029/2024gl110094, 2024.